



Pronounced zonation of seismic anisotropy in the Western Hellenic subduction zone and its geodynamic significance



Jean-Arthur Olive^{a,*}, Frederick Pearce^b, Stéphane Rondenay^c, Mark D. Behn^d

^a Massachusetts Institute of Technology/Woods Hole Oceanographic Institution Joint Program in Oceanography, Department of Geology and Geophysics, 360 Woods Hole Road, MS#24, Woods Hole, MA 02543, USA

^b Massachusetts Institute of Technology, Department of Earth, Atmospheric and Planetary Science, 77 Massachusetts Avenue, Cambridge, MA 02139, USA

^c Department of Earth Science, University of Bergen, Allegaten 41, N-5007 Bergen, Norway

^d Department of Geology and Geophysics, Woods Hole Oceanographic Institution, 360 Woods Hole Road, MS#22, Woods Hole, MA 02543, USA

ARTICLE INFO

Article history:

Received 1 October 2013

Received in revised form 14 January 2014

Accepted 21 January 2014

Available online xxxx

Editor: P. Shearer

Keywords:

seismic anisotropy

subduction zones

mantle flow

Aegean

slab rollback

serpentine

ABSTRACT

Many subduction zones exhibit significant retrograde motion of their arc and trench. The observation of fast shear-wave velocities parallel to the trench in such settings has been inferred to represent trench-parallel mantle flow beneath a retreating slab. Here, we investigate this process by measuring seismic anisotropy in the shallow Aegean mantle. We carry out shear-wave splitting analysis on a dense array of seismometers across the Western Hellenic Subduction Zone, and find a pronounced zonation of anisotropy at the scale of the subduction zone. Fast SKS splitting directions subparallel to the trench-retreat direction dominate the region nearest to the trench. Fast splitting directions abruptly transition to trench-parallel above the corner of the mantle wedge, and rotate back to trench-normal over the back-arc. We argue that the trench-normal anisotropy near the trench is explained by entrainment of an asthenospheric layer beneath the shallow-dipping portion of the slab. Toward the volcanic arc this signature is overprinted by trench-parallel anisotropy in the mantle wedge, likely caused by a layer of strained serpentine immediately above the slab. Arcward steepening of the slab and horizontal divergence of mantle flow due to rollback may generate an additional component of sub-slab trench-parallel anisotropy in this region. Poloidal flow above the retreating slab is likely the dominant source of back-arc trench-normal anisotropy. We hypothesize that trench-normal anisotropy associated with significant entrainment of the asthenospheric mantle near the trench may be widespread but only observable at shallow-dipping subduction zones where stations nearest the trench do not overlie the mantle wedge.

© 2014 Elsevier B.V. All rights reserved.

1. Introduction

Seismic anisotropy in the Earth's upper mantle is commonly attributed to the preferred alignment of olivine crystals caused by finite strain field associated with viscous flow (McKenzie, 1979). Anisotropy is measurable by quantifying the birefringence of shear waves that propagate vertically through an anisotropic layer and accumulate a time offset δt between a fast component polarized in a vertical plane of azimuth ϕ , and an orthogonal slow component (Silver and Chan, 1991). At subduction zones, two domains of anisotropy are frequently observed: a domain of trench-parallel fast directions between the trench and volcanic arc, and a domain of trench-normal directions over the back-arc (e.g., Russo and Silver, 1994; Long and Becker, 2010). Trench-normal anisotropy is commonly attributed to the lattice-preferred orientation (LPO) of

A-type olivine crystals induced by back-arc corner flow. By contrast, at subduction zones exhibiting significant slab advance or retreat, trench-parallel anisotropy is often inferred to represent trench-parallel flow driven by the trench-normal motion of the slab (Russo and Silver, 1994; Long and Silver, 2009). Such a pattern of flow, often termed toroidal, in which sub-slab mantle is forced to escape around the retreating slab and into the mantle wedge (in the case of slab retreat), has been inferred from laboratory (Buttles and Olson, 1998; Kincaid and Griffiths, 2003; Schellart, 2004; Funicello et al., 2006) and numerical (Piomallo et al., 2006; Stegman et al., 2006; Schellart et al., 2007) experiments. However, in many of those studies, toroidal flow is confined to the region near and beyond the slab edge, and it is unclear how pervasive trench-parallel flow might be beneath and above the interior portion of the slab.

Alternatively, mechanisms that do not require rollback-driven, trench-parallel sub-slab flow have been proposed to explain trench-parallel anisotropy. These mechanisms place the source of trench-parallel anisotropy within the slab or in the overlying

* Corresponding author. Tel.: +1 617 253 7278.

E-mail address: jaolive@mit.edu (J.-A. Olive).

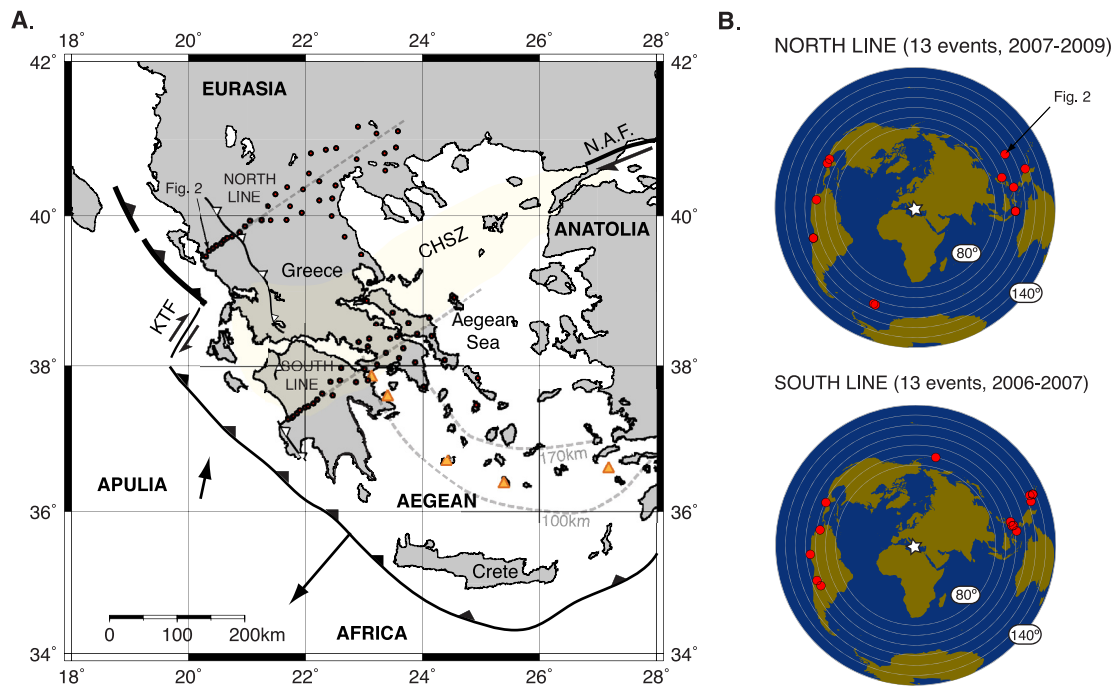


Fig. 1. A. Study area and location of the MEDUSA stations (dots). Dashed gray lines indicate the projections of the North and South lines shown on Fig. 4. The black line with barbs marks the trench in the northern segment. The thinner black line in the southern segment indicates the bathymetric trench, which is distinct from the deformation front (not shown) further to the southwest (Royden and Papanikolaou, 2011). Dashed gray curves indicate the depth to the Wadati–Benioff Zone in the Southern segment (Papazachos et al., 2000). Other major tectonic features include (Royden and Papanikolaou, 2011): the Kefalonia Transform Fault (KTF), the Central Hellenic Shear Zone (CHSZ, yellow shading), the North Anatolian Fault (NAF), the front of the internal Pindos ophiolite (thin black line with open barbs), and the active volcanic arc (orange triangles). The trench retreat velocity is indicated in a hotspot reference frame (Hatzfeld et al., 2001). The motion of Apulia in an absolute reference frame (Pérouse et al., 2012) is indicated with a black arrow. B. Teleseismic events used for SKS splitting measurements along both seismic lines. Circles are plotted every 10° of angular distance from Central Greece. The station (N002) and event (2008130) associated with the measurement shown in Fig. 2 are outlined in A and B.

fore-arc mantle wedge. Examples of such mechanisms are: serpentine-filled cracks in the downgoing slab (Faccenda et al., 2008), B-type olivine fabrics in the cold, hydrated mantle wedge nose (Jung and Karato, 2001), 3D convective instabilities (Behn et al., 2007), and flow driven by slab curvature (Kneller and van Keken, 2008). Distinguishing between these various models requires reliable constraints on the depth-distribution of the anisotropic sources, which shear-wave splitting from teleseismic arrivals does not easily provide. Splitting of local S-waves generated along the Wadati–Benioff Zone or in the slab has proven to be an effective tool to discriminate between wedge and sub-wedge anisotropy when compared with teleseismic shear wave splitting. Using this methodology, Long and Silver (2009) established that ~90% of subduction zones exhibit trench-parallel anisotropy in the sub-slab mantle. Notable exceptions featuring sub-slab trench-normal anisotropy include Cascadia (Currie et al., 2004) and Central Alaska (Christensen and Abers, 2010).

A successful model for subduction zone anisotropy must therefore account for this variability in addition to properly explaining the spatial distribution of anisotropy at the scale of individual subduction systems. It is likely that subduction zone anisotropy reflects a combination of several of the mechanisms listed above, rather than a single ubiquitous process. In particular, the geometry of a given subduction zone influences where each of these mechanisms is best expressed in measurements of seismic anisotropy, and how the anisotropy associated with these mechanisms constructively and/or destructively interferes with one another.

In this study, we attempt to isolate different sources of anisotropy based on shear-wave splitting in the Western Hellenic Subduction Zone, a subduction system experiencing significant retrograde motion of the slab (Fig. 1). Previous seismic anisotropy

studies in the region include: Pn-wave tomography (Hearn, 1999), shear-wave splitting (Hatzfeld et al., 2001; Evangelidis et al., 2011), and surface wave anisotropy (Endrun et al., 2011). These have revealed significant trench-parallel anisotropy along the Hellenic arc, as well as fast-directions parallel to the retreat of the Hellenic trench correlating well with extensional deformation throughout the back-arc domain (Jolivet et al., 2009). Here we focus on seismic anisotropy closer to the trench using a station network of unprecedented density. We show that this relatively small-scale subduction system displays pronounced zonation of anisotropy that can be attributed to the juxtaposition of several sources—each related to mantle flow or known subduction processes. We discuss our results in terms of the global variability in subduction zone anisotropy and speculate on the geodynamic implications for coupling between surface plates and the sub-asthenospheric mantle.

2. Methods

2.1. Study area: The Western Hellenic Subduction Zone

The Western Hellenic Subduction Zone (Fig. 1) is one of the small-scale (<1000 km), rapidly evolving mobile belts accommodating the slow convergence between the European and Nubian plates (Molnar, 1988; Hyndman et al., 2005; Faccenda and Becker, 2010). It displays many classical features of subduction, including a northeastward dipping slab that increases in dip from 20° to ~45° around ~100 km depth (Papazachos et al., 2000; Piromallo and Morelli, 2003; Suckale et al., 2009; Pearce et al., 2012), as well as an active volcanic arc in its southern portion. The Western Hellenic Subduction Zone is characterized by rapid southwestward retreat of the arc and trench since the late

Eocene, coincident with widespread extension in the Aegean domain (McKenzie, 1978; Le Pichon and Angelier, 1979; Dewey and Sengor, 1979). About 8–10 Myrs ago, Ionian oceanic lithosphere of Triassic or Jurassic age began to subduct along the southern portion of the trench (Royden and Papanikolaou, 2011). This led to the present-day dichotomy between the Southern Hellenides, where rapid trench retreat (30 mm/yr, southwestward with respect to Eurasia) likely expresses rapid rollback of negatively buoyant oceanic lithosphere, and the Northern Hellenides, where continental lithosphere subducts at a slower rate, and retreats by 5–10 mm/yr (Royden and Papanikolaou, 2011). Differential retreat rates are accommodated in the overriding plate along the Kefalonia Transform Fault and across the Central Hellenic Shear Zone in a more distributed fashion. These characteristics make the Western Hellenic Subduction Zone a natural laboratory for studying a range of subduction processes on a relatively small-scale system, namely: slab rollback in relation to upper-plate deformation, the dynamical effects of along-axis variation in slab buoyancy, and slab edge dynamics.

2.2. Dataset and shear wave splitting analysis

Our dataset consists of teleseismic SKS waveforms recorded by two dense arrays of broadband seismometers deployed in 2006–2009 as part of the MEDUSA experiment (Suckale et al., 2009; Pearce et al., 2012). The arrays are oriented perpendicular to the trench across the Northern and Southern Hellenides (Fig. 1), and are hereafter referred to as the North and South lines, respectively (see Supplementary Material for station coordinates). We selected waveforms originating from events of magnitude $M_w \geq 6.0$ located between 90 and 130° epicentral distance from Central Greece based on earthquake catalog information from the Preliminary Determination of Epicenters (PDE) Bulletin (USGS) (Fig. 1). The corresponding rays reached the stations with inclinations $i \leq 10^\circ$, which minimizes error in the splitting measurements due to P-to-S conversions. The actual SKS waveform was selected by visual inspection of the traces around an arrival time predicted by the IASP91 model (Kennett and Engdahl, 1991) using the TauP Toolkit (Crotwell et al., 1999). The time window employed for the measurements systematically encompassed at least one SKS period (8–10 s). All waveforms were detrended and filtered between 0.01 and 0.25 Hz to remove high-frequency noise. Waveforms characterized by a well-defined pulse of energy on the radial (R) and transverse (T) components, and displaying elliptical particle motion in (R, T) coordinates were deemed suitable for splitting analysis. We applied an eigenvalue minimization method, which consists of computing the smallest eigenvalue λ_2 of the correlation matrix of the R and T components time-shifted and rotated by trial parameters $(\delta t_T, \phi_T)$, and looking for the combination of $(\delta t_T, \phi_T) = (\delta t, \phi)$ that minimizes λ_2 . We computed error bars $(\sigma_{\delta t}, \sigma_\phi)$ around $(\delta t, \phi)$ corresponding to a 95% confidence interval, assuming that $\min(\lambda_2)$ is the sum-of-squares of a χ^2 -distributed noise process (Silver and Chan, 1991). We then corrected the SKS waveforms for the effect of splitting and validated measurements that allowed reconstruction of a radially polarized unsplit SKS wave. After correction, acceptable measurements should feature (1) little energy on the T-component and (2) linear particle motion in North–South or fast–slow coordinates (Fig. 2C–E) (i.e., no energy left on the corrected T-component). These features are assessed by visual inspection. A total of 383 acceptable splitting measurements originating from 26 events (Fig. 1; Supplementary Table S3) were recovered, and are listed in Supplementary Tables S4 (North line) and S5 (South line). To further assess the quality of our measurements, we computed a signal-to-noise ratio (SNR) using the T-component of the SKS waveform and a window of the same length immediately preceding it. An example of our splitting

methodology is illustrated in Fig. 2 for an SKS waveform originating from a Philippine trench earthquake recorded on the North line (Fig. 1).

Monteiller and Chevrot (2010) recently showed that individual splitting measurements do not provide reliable estimates of single-station anisotropy, particularly when SKS energy is weak or moderate on the transverse component, which is often the case in our dataset. We therefore computed average SKS splitting parameters for each station following the stacking procedure of Wolfe and Silver (1998), which has been shown to yield unbiased, robust estimates of single-station anisotropy (Monteiller and Chevrot, 2010). At all stations that yielded at least two acceptable SKS splitting measurements, we stacked the $\lambda_2/\min(\lambda_2)$ maps (Fig. 2B) from each measurement, and computed $(\delta t, \phi)$ and a 95% confidence interval using the resulting map of stacked- λ_2 normalized by its minimal value. This method weights more heavily the measurements that feature better-pronounced minima. These generally correspond to waveforms that have higher SNR. We therefore did not invalidate any measurement based on a low SNR, but instead relied on the stacking method to automatically assign little weight to low-SNR measurements. Stacked parameters are listed in Supplementary Tables S4 and S5 for the North and South lines, respectively. In the case of depth-dependent anisotropy, these tend to be more sensitive to the shallowest/strongest anisotropic source (Monteiller and Chevrot, 2010).

3. Results

3.1. Three distinct anisotropy domains

The stacked splitting parameters recovered from our analysis outline three distinct domains of anisotropy (Fig. 3): near-trench (NT), fore-arc (FA), and back-arc (BA). The NT domain (within 120–150 km of the trench along either line) is characterized by trench-oblique/normal fast-directions averaging $N021^\circ \pm 12^\circ$ (standard deviation) in the North (based on a number of station averages $n = 8$) and $N058^\circ \pm 11^\circ$ ($n = 4$) in the South. Within this domain, delay times decrease almost linearly from 1.0 to 0.5 s with increasing distance from the trench along the North (and possibly South) line (Fig. 4A, 4B). The most trench-oblique NT fast azimuths are found in the North line, where they trend sub-parallel to the Kefalonia Transform Fault (Fig. 3), which marks the surface expression of the differential retreat between the Northern and Southern Hellenides (Royden and Papanikolaou, 2011). A directional V-test (Berens, 2009) overwhelmingly rejects the hypothesis that NT fast-directions are uniformly distributed ($p = 2.8 \times 10^{-6}$, $n = 12$, see Supplementary material for details), and favors the alternative hypothesis that they are drawn from a distribution that averages $N040^\circ$, which corresponds to the mean direction of rapid trench retreat in the Southern segment in a hotspot reference frame (Hatzfeld et al., 2001). By contrast, the motion of the subducting plate in an absolute reference frame is slower (~ 1 cm/yr) and oriented $N010^\circ$ (Pérouse et al., 2012). The NT domain transitions over a distance of less than 20 km into the FA domain, where fast-directions are predominantly trench-parallel, averaging $N127^\circ \pm 22^\circ$ and $N157^\circ \pm 15^\circ$ in the North ($n = 15$) and South ($n = 9$) lines, respectively. Along the South line, the trenchward half of the FA stations yield a high proportion of null-measurements indicating a wide range of possible fast-azimuths (Supplementary Tables S4 and S5). Delay times over the entire FA domain are moderate (0.74 ± 0.21 s) and more scattered than in other domains. Farthest to the east in the BA domain, SKS fast directions transition sharply back to trench-normal. This transition occurs ~ 275 km from the trench in the South line (~ 25 km northeastward of the active volcanic arc), which

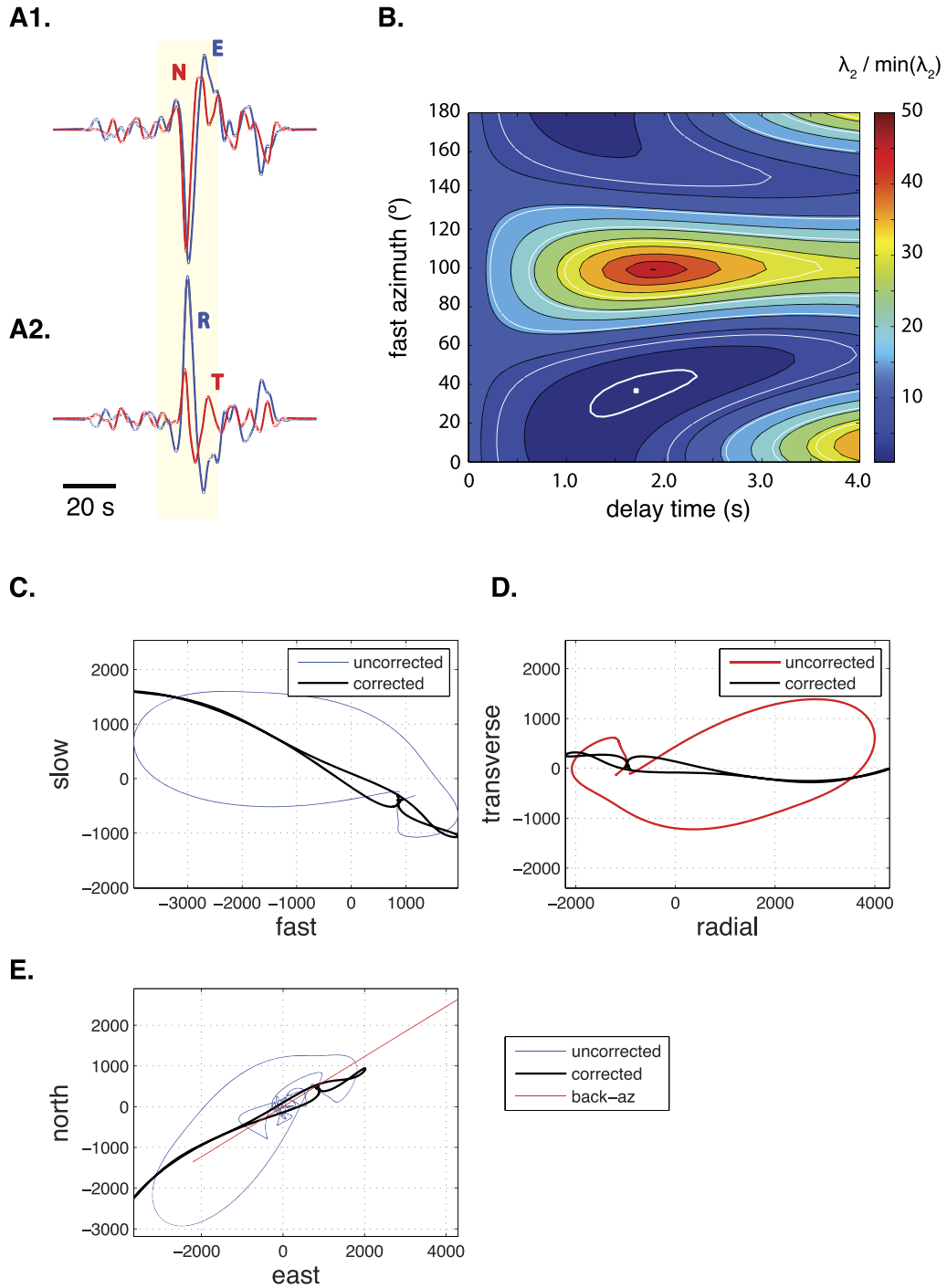


Fig. 2. Example SKS splitting measurement. This example corresponds to event 2008130 (Fig. 1B) recorded at station N002 (NT domain, Fig. 1A). A1–A2. Filtered traces in N–S/E–W and R/T coordinates, respectively. B. Map of $\lambda_2 / \min(\lambda_2)$ showing the best estimate of $(\delta t, \phi)$ (white dot) circled by the 95% confidence contour (white line). C–D–E. Particle motion plots of the uncorrected (recorded) and corrected (unsplit) SKS waveforms in various coordinates (fast and slow anisotropic directions, R/T and N/E). Unsplitting the SKS waveform yields a radially polarized wave: particle motion becomes linear (C), shows no energy on the transverse component (D) and aligns with the wave back-azimuth (E).

is consistent with previous observations (Hatzfeld et al., 2001; Evangelidis et al., 2011). A similar transition to trench-normal anisotropy is observed ~ 380 km from the trench in the North line, despite the absence of a presently active volcanic arc in this region.

3.2. Constraints on the depth-distribution of anisotropy

To assess the depth-distribution of anisotropy, we compare our SKS splitting results with two co-located Generalized Radon Trans-

form (GRT) images computed from scattered teleseismic S waves (Suckale et al., 2009; Pearce et al., 2012) (Fig. 4C, 4F). These images outline the subducting crust and Moho of the overriding plate (Suckale et al., 2009; Pearce et al., 2012). A remarkable result is that for both lines, the sharp rotation in anisotropy between the NT and FA domains occurs almost directly above the tip of the mantle wedge, where the top of the slab intersects the Moho of the overriding plate (Fig. 4). This suggests that the FA anisotropy has a significant mantle wedge component. While

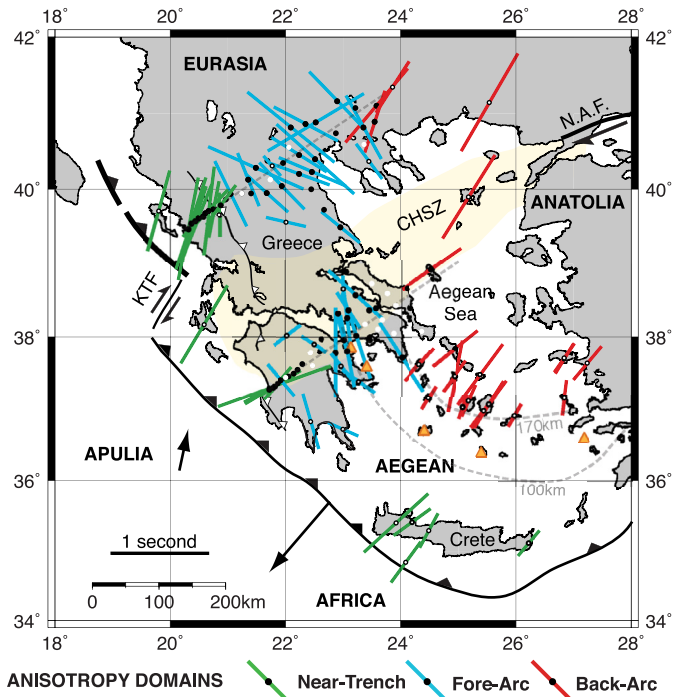


Fig. 3. Stacked SKS splitting parameters at MEDUSA stations (black circles, this study) and from prior studies (open circles, Evangelidis et al., 2011). See Fig. 1 caption for symbols. The motion of Apulia in an absolute reference frame (Pérouse et al., 2012) is indicated with a black arrow. Stations featuring only null measurements are indicated as black circles. The corresponding individual measurements are shown in Fig. 4.

a contribution from a deeper trench-parallel anisotropy source cannot be ruled out, it would be less likely to generate an abrupt NT-FA transition than a shallow source because of the broadening of the SKS Fresnel zone with depth. A corollary to this result is that the anisotropy recorded in the NT domain does not originate in the mantle wedge. It is also unlikely that it originates in the thick overriding crust-on-subducting crust section imaged beneath the NT, given that a 50-km crustal section with 1–2% anisotropy, as inferred from surface waves (Endrun et al., 2011), would generate only 0.1–0.3 s of splitting. Additionally, Pn-anisotropy (Hearn, 1999) reveals trench-parallel to North-South fast-directions in the NT domain likely originating at subducting Moho depths, inconsistent with our SKS fast directions. The fact that trench-oblique/normal fast-directions are observed along both the South and North lines, where geologically distinct lithospheres enter the system (Royden and Papanikolaou, 2011; Pearce et al., 2012) does not support a lithospheric (subducting) mantle origin for NT anisotropy. This is consistent with recent observations of a weakly anisotropic Ionian lithosphere subducting in Calabria (Baccheschi et al., 2011). The most plausible interpretation for NT fast-directions sub-parallel to the trench retreat direction is therefore that they originate in the sub-slab asthenosphere, and represent LPO of A-type olivine induced by trench-normal finite strain beneath the downgoing, retreating slab. We favor a similar interpretation for the BA anisotropy, involving trench-normal strain in the mantle overlying the subducting slab (Jolivet et al., 2009; Brun and Sokoutis, 2010; Endrun et al., 2011; Evangelidis et al., 2011). A schematic summary of the constraints on the depth-distribution of anisotropy discussed above is presented in Fig. 5.

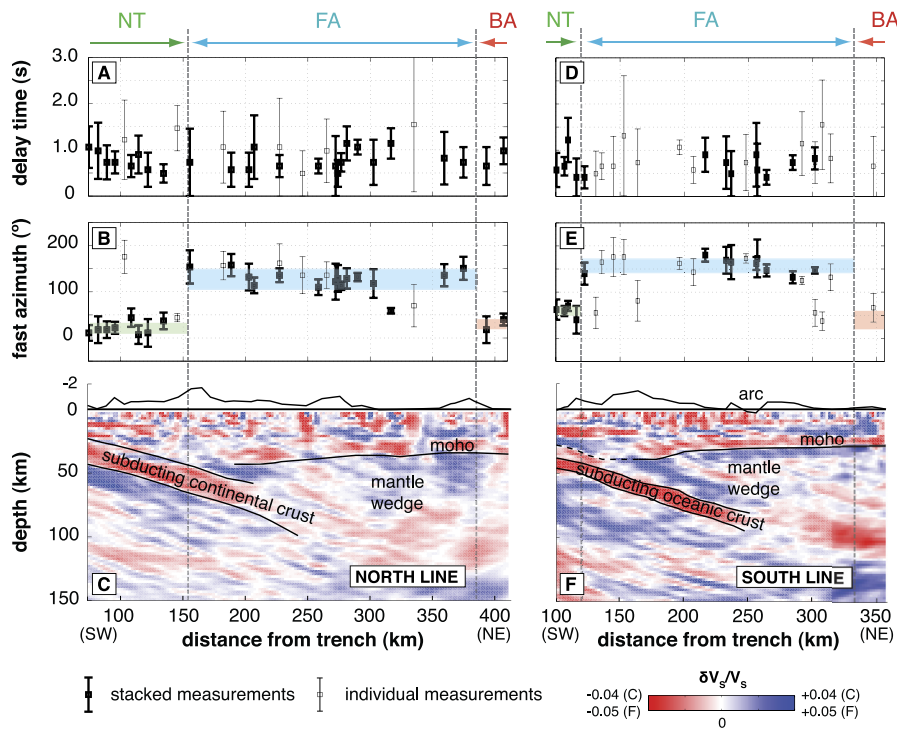


Fig. 4. Splitting parameters (stacked, bold black squares) projected along the two trench-perpendicular lines (Fig. 1). A, B: North line; D, E: South line. Individual splitting measurements are given as open squares at stations where stacked parameters could not be computed. Colored rectangles indicate the mean fast-azimuth \pm its 1- σ standard deviation for each domain. C, F: 2-D images of S-wave velocity perturbations computed from migration of scattered teleseismic S waves, with geologic interpretation, for the North and South lines, respectively (modified from Pearce et al., 2012). Topography along the lines is plotted above each image. The boundaries of each anisotropy domain as defined on Fig. 3 are indicated with dashed lines.

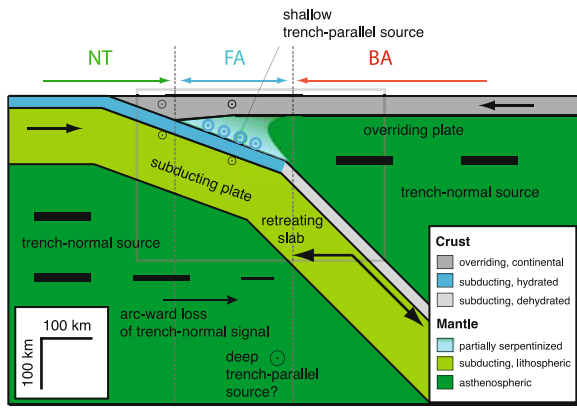


Fig. 5. Schematic summary of the resolved depth-distribution of seismic anisotropy in the Western Hellenic subduction zone. Dotted circles and horizontal bars represent trench-parallel and trench-normal anisotropy, respectively. The location of the images from Fig. 4C and 4F is shown as a gray rectangle. The geometry and nature of the subducting and overriding crust follows the interpretation of Pearce et al. (2012). The shallow trench-parallel anisotropy indicated as thin black circles is inferred from the surface wave study of Endrun et al. (2011) and the Pn-anisotropy study of Hearn (1999).

4. Geodynamic interpretation

4.1. Seismic anisotropy induced above and beneath a retreating slab

In this section we discuss our results in the context of previous numerical and analog studies of mantle flow around a retreating slab. We first focus on the generic, robust flow patterns that arise beneath and above a homogeneous slab undergoing rollback, and their seismic anisotropy signature. Adjustments to the generic models that are relevant to the Hellenic subduction zone will be further discussed in Section 4.3. Tank experiments (Buttles and Olson, 1998; Kincaid and Griffiths, 2003; Schellart, 2004; Funicello et al., 2006) and 3D numerical models (Piomallo et al., 2006; Stegman et al., 2006; Schellart et al., 2007; Faccenda and Capitanio, 2012; Li and Ribe, 2012) predict that flow beneath a retreating slab is strongly coupled to the surrounding asthenosphere and should be dominantly trench-normal (poloidal) beneath the interior of the slab and show a strong toroidal component (return flow) near and beyond the slab edges. This contrasts

with models that include a thin low viscosity decoupling layer immediately beneath the slab, which enhances the sub-slab, trench-parallel component of flow (Long and Silver, 2009). However, the relationship between flow direction and seismic anisotropy is not straightforward. Faccenda and Capitanio (2012, 2013) modeled the development of LPO in olivine–enstatite aggregates advected in a 3D slab rollback flow field. They established that the supra-slab domain should be dominated by trench-normal anisotropy due to simple shear in the flow entrained by the retreating slab. Further, they found two distinct regions of anisotropy in the sub-slab domain (Fig. 6A). At shallow levels, simple shear beneath the slab generates a layer of trench-normal fast axes. The thickness of this layer is on the order of 100 km, but may be thicker beneath wider slabs that drive a stronger poloidal flow component. At greater depths within this entrained layer, the fast axes remain trench-normal but plunge parallel to the slab. Faccenda and Capitanio (2012, 2013) found that this layer systematically overlies a deeper layer, or “core” of trench-parallel fast-axes, which is generated by pure-shear in the slab retreat direction. This anisotropic core is strongest near the slab edges, where the divergence of the horizontal sub-slab flow is greatest. Beneath the interior portion of the slab, the deep trench-parallel anisotropy is weak, and SKS fast-azimuths largely reflect the shallower trench-normal layer. Closer to the slab edge, the stronger trench-parallel core starts to destructively interfere with the shallow trench-normal layer, yielding short SKS delay times. Near and beyond the slab edges, simple shear aligns the olivine fast-axes parallel to the toroidal (return) flow (Fig. 6A). The toroidal flow seems to disrupt the trench-normal anisotropy both above and below the slab interior over a horizontal distance from the slab edge that is comparable to 2–3 times the slab width, resulting in trench-oblique SKS fast azimuths close to the slab edge.

The Faccenda and Capitanio (2013) model is consistent with our observation of strongly expressed trench-normal anisotropy in the BA and NT domains (Figs. 3, 6). NT anisotropy could indeed reflect a shallow sub-slab layer of entrained asthenospheric mantle, while BA anisotropy could reflect its supra-slab counterpart. If this is the case, then the sub-slab trench-normal layer should not be confined to the NT domain and should extend northeastward beneath the FA domain. As we discussed in Section 3.2 the abrupt transition between trench-normal and trench-parallel anisotropy above the tip of the mantle wedge strongly suggests that the trench-parallel

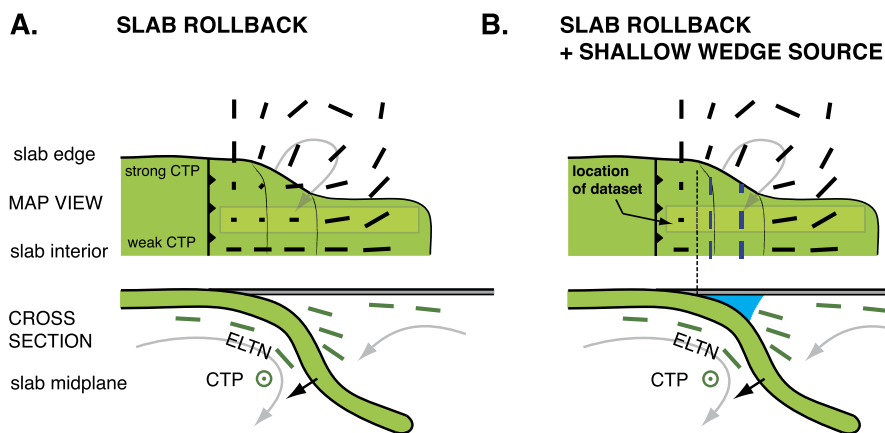


Fig. 6. Conceptual model for the zonation and depth-distribution of anisotropy above and below a retreating slab. A. Main features from the Faccenda and Capitanio (2013) model (see Section 4.1 for details). Mantle flow is shown as gray arrows, olivine fast-axes as green bars/dotted circles, and the resulting SKS splitting measurements as black bars on the map view. The upper sub-slab domain consists in an entrained layer of trench-normal fast-axes (ELTN) overlying a deeper core of trench-parallel fast-axes (CTP). The CTP is best expressed near the slab edge, where it destructively interferes with the ELTN to yield weak SKS splitting (black bars). Beneath the slab interior, the ELTN dominates the signal and generates trench-normal fast SKS azimuths. Beyond the slab edge, SKS fast-azimuths outline the toroidal pattern of the return flow. B. Same as A, with an additional mantle wedge source of trench-parallel anisotropy (e.g., a supra-slab layer of sheared serpentine). This additional component disrupts the SKS splitting pattern (blue bars) and results in the formation of three distinct regions of anisotropy, similar to what is observed in the Western Hellenic Subduction Zone.

FA anisotropy must have a strong mantle wedge component. This component (whose nature will be discussed in Section 4.2) may destructively interfere with an underlying trench-normal layer, accounting for the large proportion of null measurements in the trench-ward half of the FA domain. Further, the observed arc-ward decrease in delay times in the NT domain (Fig. 4A, 4D) may be indicative of a diminishing expression of the sub-slab trench-normal layer as one moves away from the trench. The Faccenda and Capitanio (2012, 2013) models provide two possible explanations for the waning contribution of sub-slab trench-normal anisotropy arc-ward from the trench. One is the arc-ward steepening of the olivine *a*-axes parallel to the steepening Hellenic slab, which would result in shorter associated SKS delay times. The other is destructive interference between the trench-normal sub-slab layer and an even deeper trench-parallel core, which would be situated beneath the arc-ward portion of the FA domain.

4.2. Anisotropy in the fore-arc portion of the mantle wedge

As discussed above, FA trench-parallel fast-directions likely originate in the mantle wedge, and are well expressed even in the thinnest portion of the wedge (Figs. 4, 5). Jung and Karato (2001) and Kneller et al. (2005; 2007) have proposed that B-type olivine fabrics formed under hydrous high-stress/low-temperature conditions expected near the tip of the mantle wedge could produce such trench-parallel fast directions when sheared in a trench-normal flow. Alternatively, trench-parallel flow (Long and Silver, 2009) or trench-parallel stretching due to slab curvature (Kneller and van Keken, 2008) could generate trench-parallel fast-azimuths if A-type olivine constitutes the prevalent wedge fabric. All these mechanisms would, however, predict a correlation between wedge thickness and delay time over the NT domain, which is not observed.

Thus, we prefer an alternative model in which the trench-parallel fast directions reflect LPO in a thin layer of serpentine located immediately above the subducting slab and sheared in a trench-normal direction (Katayama et al., 2009; Jung, 2011; Wagner et al., 2013). Such a layer could generate split times of 1 s with a thickness of only ~10 km, allowing it to be well expressed in the SKS measurements even in the thin mantle wedge “nose”.

4.3. Implications for the Hellenic subduction system

Our results are best explained by a model that combines (1) a shallow mantle wedge source of trench-parallel anisotropy (e.g., a thin supra-slab layer of serpentine), which is primarily sampled over the FA domain, and (2) rollback-driven finite strain, which is primarily sampled over the NT and BA domain (Fig. 6B). This model is compatible with the hypothesis that the negative buoyancy of the Hellenic slab drives widespread south-westward asthenospheric flow (Faccenna and Becker, 2010) potentially linked to the extensional deformation of the overriding plate (Jolivet et al., 2009). Further, our data suggests that the sub-slab flow field is largely trench-normal beneath the slab interior and that the trench-parallel anisotropy originates in the mantle wedge. This contrasts with previous interpretations of sparser anisotropy measurements invoking widespread trench-parallel flow of mantle escaping beneath the slab interior to accommodate the retreat of the Hellenic slab (Jolivet et al., 2009; Brun and Sokoutis, 2010; Evangelidis et al., 2011). It is possible that the along-trench variation in slab buoyancy between the Northern and Southern segments drives a component of sub-slab trench-parallel flow (Capitanio and Faccenda, 2012). However, recent models incorporating differential retreat rates due to along-trench buoyancy

gradients predict fast-SKS azimuths dominantly parallel to the retreat motion and no strong trench-parallel anisotropy (Faccenda and Capitanio, 2013). We therefore favor a model in which the return (locally trench-parallel) flow from the sub-slab to the supra-slab domain is confined to near (<100 km, Kneller and van Keken, 2008) and beyond the slab edges. In the framework of the Faccenda and Capitanio (2013) study, the slight obliquity of the NT fast-azimuths in the Northern Hellenides may be indicative of proximity to the northern slab edge. If this is the case, we expect that shear wave splitting measurements carried out further North (around 42°N) would image the toroidal flow pattern around the northern slab edge in a fashion similar to what is observed south of the Cascadia subduction zone (Zandt and Humphreys, 2008). Such a study would help resolve the debate on whether the true Northern edge of subduction (around which asthenospheric return flow takes place) is in the North of the Northern Hellenides, or between the Southern and Northern Hellenides.

Several authors have suggested that the differential retreat rates between the Northern and Southern Hellenides could be accommodated by a slab tear. While some studies advocate a vertical tear that would trend parallel to the Kefalonia Transform (e.g., Royden and Papanikolaou, 2011), others propose a horizontal tear propagating southward toward the most negatively buoyant portions of the slab (e.g., Spakman et al., 1988; Wortel and Spakman, 2000). Seismic imaging supports a continuous transition between the subducting lithospheres in the Northern and Southern segments at depths shallower than 100 km (Pearce et al., 2012), but cannot rule out a deeper tear coincident with the transition between oceanic and continental subducting crust. Suckale et al. (2009) argued that such a tear could account for the significant three-dimensionality they found in supra-slab mantle properties. If such a tear existed, it would accommodate about 100 km of differential retreat (Royden and Papanikolaou, 2011), which is commensurate with the effective elastic thickness of the subducting lithosphere in both segments (~70 km, Royden, 1993; Pearce et al., 2012). It is therefore unlikely that such a tear would allow a large inflow of asthenosphere through the slab, and therefore induce a fully developed return flow beneath the Central Hellenic Shear Zone (Fig. 3). Such a return flow would cause a strong asymmetry in seismic anisotropy with respect to the Central Hellenic Shear Zone, with a toroidal pattern in the fast-SKS azimuths over the Northern Hellenides, which is not observed. Further, the remarkable similarity between the anisotropy distribution in the Northern and Southern Hellenides in spite of the present-day slow trench retreat in the North suggests (1) some degree of along-trench continuity in the processes that cause anisotropy (i.e., mantle strain) and (2) that the anisotropy zonation was acquired >10 Myrs ago when the entire system was uniformly retreating (Royden and Papanikolaou, 2011). Alternatively, it could indicate ongoing rollback of the deeper portion of the slab beneath the Northern Hellenides, which is not expressed in the surface GPS velocities.

4.4. New constraints for the interpretation of seismic anisotropy at subduction zones

Our study reports a new occurrence of sub-slab trench-normal anisotropy in close proximity to the trench. This contrasts with the observation of sub-slab trench-parallel anisotropy at ~90% of subduction zones worldwide (Long and Silver, 2009; Foley and Long, 2011). Interestingly, the numerical models of Faccenda and Capitanio (2013) predict two sub-slab domains of anisotropy. The upper sub-slab domain typically features strong trench-normal anisotropy driven by the advance of the subducting plate, while the lower sub-slab domain features trench-parallel fabrics induced by pure shear in the slab retreat direction. Faccenda and Capitanio

(2013) further argue that the deeper trench-parallel anisotropy should be better expressed in subduction systems with limited along-trench extent and/or displaying faster trench migration than plate subduction. The Western Hellenic Subduction Zone displays both of these characteristics, and yet shows well expressed sub-slab trench-normal anisotropy in the NT domain. However, we cannot rule out the possibility of sub-slab trench-parallel fabrics closer to the arc that could contribute to the anisotropy in the FA domain.

It is noteworthy that the Nazca, Juan de Fuca, Rivera, Pacific (beneath Alaska) and Hellenic slabs, which all display trench-normal anisotropy in the NT domain (Polet et al., 2000; Currie et al., 2004; Soto et al., 2009; Christensen and Abers, 2010; Hicks et al., 2012), have a shallow-dipping slab ($<35^\circ$) near the trench. This allows land-based stations to sample a portion of the NT domain that does not overlie the mantle wedge, and thus provide a direct window with which to investigate the sub-slab asthenosphere. By contrast, more steeply dipping slabs would result in the trench-parallel mantle wedge signal being expressed immediately arc-ward of the trench, perhaps inhibiting the formation of a clear NT zone of trench-normal anisotropy. We therefore propose that sub-slab trench-normal anisotropy could be more widespread than previously thought, but only observable at stations that are close enough to the trench, or beneath slabs that have a shallow-dipping portion. A steeper slab would also result in steeply dipping trench-normal fast-axes immediately beneath the slab, which would limit their contribution to the splitting of SKS waves, and allow the underlying trench-parallel sub-slab core to be better expressed. This model could be tested by future studies using ocean bottom seismometers to extend SKS datasets seaward of the trench toward the outer rise.

Among the few subduction zones that feature NT trench-normal anisotropy, Alaska is perhaps the one that allows the most pertinent comparisons with the Western Hellenic Subduction Zone. Alaska features a rapid transition from well-expressed trench-normal anisotropy near the trench to trench-parallel anisotropy near and beyond the volcanic arc (Christensen and Abers, 2010). This transition appears most abrupt in map view when splitting measurements are relocated to depths greater than 50 km along the SKS ray path. Further, the transition roughly correlates with the onset of a high-attenuation region of the mantle wedge, and the trench-parallel delay times generally increase with wedge thickness. Christensen and Abers (2010) therefore proposed an interpretation similar to our model for the Hellenic Subduction, in which FA trench-parallel anisotropy in the wedge overpowers a sub-slab source of trench-normal anisotropy that is best expressed near the trench. They attributed wedge anisotropy to trench-parallel flow distributed throughout the high-attenuation portions of the wedge. We cannot propose the same interpretation for the Western Hellenic subduction due to (1) the lack of correlation between delay times and wedge thickness, and (2) the observation of robust trench-parallel anisotropy even in the thin mantle wedge nose, which is unlikely to develop strongly anisotropic fabrics through mantle flow (Kneller et al., 2007).

A recent study by Song and Kawakatsu (2012) pointed out that orthorhombic symmetry combining azimuthal and strong radial anisotropy constitutes a more realistic model for asthenospheric LPO than transverse isotropy (Silver and Chan, 1991). Under this assumption, Song and Kawakatsu (2012) showed that trench-normal fast axes would only generate trench-normal fast SKS splitting if the fast axes are dipping at a shallow angle ($<15^\circ$). More steeply dipping fast-axes would instead produce sub-slab trench-parallel SKS splitting. This result has important implications on how the entrained sub-slab layer of trench-normal fast-axes would be expressed as fast SKS azimuths. It suggests that as the entrained layer steepens parallel to the slab dip, a transition from

trench-normal to trench-parallel anisotropy would occur beneath the slab. Following this approach, Song and Kawakatsu (2012, 2013) proposed that the anisotropy rotation observed in Alaska reflects the progressive steepening of a sub-slab asthenospheric layer with strong radial anisotropy entrained beneath a steepening slab and sheared in a trench-normal direction. Their model accounts for the back-azimuthal dependence of the splitting directions while correctly predicting the measured delay times (underestimated by the Christensen and Abers (2010) model, even when considering strong wedge anisotropy), as well as the increase in delay times away from the trench. Interestingly, the Song and Kawakatsu (2013) model provides an explanation for sub-slab trench-parallel anisotropy that does not require strong lateral motion of the trench (retreat or advance), which is a characteristic of the Alaskan subduction (Schellart et al., 2011). It is unclear, however, to what extent the Song and Kawakatsu (2012, 2013) model can explain the abruptness of the transition between trench-normal and trench-parallel anisotropy beneath the progressively steepening Alaskan slab, as the model predicts a smooth rotation of the fast axes with increasing slab dip.

In the Western Hellenic subduction zone the change in slab dip from 20 to 45° is potentially more abrupt and occurs at a depth of ~ 100 km (Papazachos et al., 2000; Piromallo and Morelli, 2003; Suckale et al., 2009; Pearce et al., 2012). If the entrained sub-slab layer of trench-normal fast axes predicted by the Faccenda and Capitanio (2012, 2013) models undergoes commensurate steepening, it could constitute a sub-slab source of trench-parallel anisotropy with an abrupt onset arc-ward of the 100 km slab depth contour, complementing trench-parallel anisotropy originating in the mantle wedge and perhaps at greater sub-slab depths (Fig. 6B) in the FA domain. This would be consistent with the better-expressed trench-parallel anisotropy beneath the arc-ward portion of the FA domain in the Western Hellenic Subduction Zone, but cannot explain the abrupt NT-FA transition, which occurs trench-ward of the 100 km slab depth contour (Fig. 3). This model requires strong radial anisotropy in the subducting asthenosphere, which is characteristic of the asthenosphere beneath most oceanic plates (e.g., Nishimura and Forsyth, 1989). In the Hellenic subduction, the subducting asthenosphere is not well characterized due to its complex history and heterogeneity (juxtaposition of oceanic and continental microplates). However, lateral slab motion could promote the development of strong radial anisotropy in the subducting asthenosphere through pure shear beneath the slab, especially in such a small-scale subduction system (Song and Kawakatsu, 2012, 2013). Finally, we note that the back-azimuthal dependence of our individual splitting measurements (Supplementary material) in the NT domain does not appear consistent with the Song and Kawakatsu (2012) model. However, the back-azimuthal dependence likely reflects a range of complex mechanisms that are difficult to deconvolve from one another. Those include a pronounced layering of anisotropy with a complex geometry (dipping layers with three-dimensional geometries) as well as strong heterogeneity in the anisotropic fabrics.

5. Conclusions

We present new shear-wave splitting measurements on a dense station network in the Western Hellenic Subduction Zone, a small-scale subduction system undergoing slab rollback. We interpret trench-normal fast-azimuths in the near-trench and back-arc domains as indicative of sub-slab and supra-slab trench-normal fast-axes (respectively), both induced by rollback-driven mantle flow. We argue that most of the trench-parallel anisotropy observed in the fore-arc domain originates in the mantle wedge and locally overprints the rollback-induced anisotropy. Our interpretation suggests that the retreating slab is mechanically coupled to the

surrounding mantle, and entrains significant volumes of asthenosphere towards the base of the upper-mantle. This contrasts with a frequently proposed alternative model where a weak decoupling layer forms beneath the sinking slab, allowing sub-slab mantle to escape horizontally through trench-parallel flow.

We further suggest that while similar mantle flow patterns can be expected at most retreating subduction zones, their anisotropic expression may be strongly modulated by the local slab dip. Specifically, it is possible that most subduction zones feature both a shallow region of trench-normal anisotropy and a deeper region of trench-parallel anisotropy beneath the slab. At subduction zones characterized by a shallow-dipping slab portion (e.g., Cascadia, the Western Hellenic Subduction Zone) it may be easier to sample the shallow trench-normal anisotropy with land-based stations. At the majority of subduction zones, however, a steep slab would result in a poorly expressed trench-normal layer overlying a deep trench-parallel layer immediately beneath the fore-arc domain, thereby promoting well-expressed trench-parallel sub-slab anisotropy. These predictions should motivate future high-resolution studies of anisotropy with methods that can resolve depth-variations (e.g., surface waves), and detailed comparisons of the anisotropy zonation at various subduction settings.

Acknowledgements

We thank the National Observatory of Athens and IRIS-PASSCAL for facilitating the fieldwork and providing the seismic instruments. We thank N. Ribe for fruitful discussions, and E. Mittelstaedt for assistance with figures. Funding was provided by NSF Continental Dynamics grant EAR-0409373 as part of project MEDUSA (F.P., S.R.), and EAR-0854673 (J.-A.O., M.D.B.).

Appendix A. Supplementary material

Supplementary material related to this article can be found online at <http://dx.doi.org/10.1016/j.epsl.2014.01.029>.

References

- Baccheschi, P., Margheriti, L., Steckler, M.S., Boschi, E., 2011. Anisotropy patterns in the subducting lithosphere and in the mantle wedge: A case study – The southern Italy subduction system. *J. Geophys. Res.* 116 (B08306). <http://dx.doi.org/10.1029/2010JB007961>.
- Behn, M.D., Hirth, G., Kelemen, P.B., 2007. Trench-parallel anisotropy produced by foundering of arc lower crust. *Science* 317. <http://dx.doi.org/10.1126/science.1141269>.
- Berens, P., 2009. CircStat: A MATLAB toolbox for circular statistics. *J. Stat. Softw.* 31 (10).
- Brun, J.P., Sokoutis, D., 2010. 45 m.y. of Aegean crust and mantle flow driven by trench retreat. *Geology* 38 (9), 815–818.
- Buttles, J., Olson, P.A., 1998. A laboratory model of subduction zone anisotropy. *Earth Planet. Sci. Lett.* 164, 245–262.
- Capitanio, F.A., Faccenda, M., 2012. Complex mantle flow around heterogeneous subducting oceanic plates. *Earth Planet. Sci. Lett.* 353, 29–37. <http://dx.doi.org/10.1016/j.epsl.2012.07.042>.
- Christensen, D.H., Abers, G.A., 2010. Seismic anisotropy under central Alaska from SKS splitting observations. *J. Geophys. Res.* 115. <http://dx.doi.org/10.1029/2009JB006712>.
- Crotwell, H.P., Owens, T.J., Ritsema, J., 1999. The TauP toolkit: flexible seismic travel-time and ray-path utilities. *Seismol. Res. Lett.* 70 (2), 154–160.
- Currie, C.A., Cassidy, J.F., Hyndman, R.D., Bostock, M.G., 2004. Shear wave anisotropy beneath the Cascadia subduction zone and western North American craton. *Geophys. J. Int.* 157, 341–353.
- Dewey, J.F., Sengor, C., 1979. Aegean and surrounding regions: Complex multiplate and continuum tectonics in a convergent zone. *Geol. Soc. Am. Bull.* 90 (1), 84–92. [http://dx.doi.org/10.1130/0016-7606\(1979\)90<84:AASRCM>2.0.CO;2](http://dx.doi.org/10.1130/0016-7606(1979)90<84:AASRCM>2.0.CO;2).
- Endrun, B., Lebedev, S., Meier, T., Tirel, C., Friederich, W., 2011. Complex layered deformation within the Aegean crust and mantle revealed by seismic anisotropy. *Nat. Geosci.* 4. <http://dx.doi.org/10.1038/ngeo1065>.
- Evangelidis, C.P., Liang, W.-T., Melis, N.S., Konstantinou, K.I., 2011. Shear wave anisotropy beneath the Aegean inferred from SKS splitting observations. *J. Geophys. Res.* 116. <http://dx.doi.org/10.1029/2010JB007884>.
- Faccenda, M., Burlini, L., Gerya, T.V., Mainprice, D., 2008. Fault-induced seismic anisotropy by hydration in subducting oceanic plates. *Nature* 455. <http://dx.doi.org/10.1038/nature07376>.
- Faccenda, M., Capitanio, F.A., 2012. Development of mantle seismic anisotropy during subduction-induced 3-D flow. *Geophys. Res. Lett.* 39. <http://dx.doi.org/10.1029/2012GL051988>.
- Faccenda, M., Capitanio, F.A., 2013. Seismic anisotropy around subduction zones: Insights from three-dimensional modeling of upper-mantle deformation and SKS splitting calculations. *Geochem. Geophys. Geosyst.* 14. <http://dx.doi.org/10.1029/2012GC004451>.
- Faccenna, C., Becker, T.W., 2010. Shaping mobile belts by small-scale convection. *Nature* 465. <http://dx.doi.org/10.1038/nature09064>.
- Foley, B.J., Long, M.D., 2011. Upper and mid-mantle anisotropy beneath the Tonga slab. *Geophys. Res. Lett.* 38. <http://dx.doi.org/10.1029/2010GL046021>.
- Funciello, F., Moroni, M., Piromallo, C., Faccenna, C., Cenedese, A., Bui, H.A., 2006. Mapping mantle flow during retreating subduction: Laboratory models analyzed by feature tracking. *J. Geophys. Res.* 111. <http://dx.doi.org/10.1029/2005JB003792>.
- Hatzfeld, D., Karagianni, E., Kassaras, I., Kiratzi, A., Louvari, E., Lyon-Caen, H., Makropoulos, K., Papadimitriou, P., Bock, G., Priestley, K., 2001. Shear wave anisotropy in the upper mantle beneath the Aegean related to internal deformation. *J. Geophys. Res.* 106 (12), 30737–30753.
- Hearn, T.M., 1999. Uppermost mantle velocities and anisotropy beneath Europe. *J. Geophys. Res.* 104 (B7), 15123–15139.
- Hicks, S.P., Nippres, S.E.J., Rietbrock, A., 2012. Sub-slab mantle anisotropy beneath south-central Chile. *Earth Planet. Sci. Lett.* 357, 203–213. <http://dx.doi.org/10.1016/j.epsl.2012.09.017>.
- Hyndman, R.D., Currie, C.A., Mazzotti, S., 2005. Subduction zone backarcs, mobile belts, and orogenic heat. *GSA Today* 15. [http://dx.doi.org/10.1130/1052-5173\(2005\)015](http://dx.doi.org/10.1130/1052-5173(2005)015).
- Jolivet, L., Faccenna, C., Piromallo, C., 2009. From mantle to crust: Stretching the Mediterranean. *Earth Planet. Sci. Lett.* 285, 198–209. <http://dx.doi.org/10.1016/j.epsl.2009.06.017>.
- Jung, H., 2011. Seismic anisotropy produced by serpentine in the mantle wedge. *Earth Planet. Sci. Lett.* 307, 535–543.
- Jung, H., Karato, S., 2001. Water-induced fabric transitions in olivine. *Science* 293. <http://dx.doi.org/10.1126/science.1062235>.
- Katayama, I., Hirauchi, K., Michibayashi, K., Ando, J., 2009. Trench-parallel anisotropy produced by serpentine deformation in the hydrated mantle wedge. *Nature* 461. <http://dx.doi.org/10.1038/nature08513>.
- Kennett, B.L.N., Engdahl, E.R., 1991. Traveltimes for global earthquake location and phase identification. *Geophys. J. Int.* 105 (2), 429–465.
- Kincaid, C., Griffiths, R.W., 2003. Laboratory models of the thermal evolution of the mantle during rollback subduction. *Nature* 425. <http://dx.doi.org/10.1038/nature01923>.
- Kneller, E.A., van Keken, P.E., Karato, S.I., Park, J., 2005. B-type olivine fabric in the mantle wedge: Insights from high-resolution non-Newtonian subduction zone models. *Earth Planet. Sci. Lett.* 237, 781–797.
- Kneller, E.A., van Keken, P.E., Katayama, I., Karato, S.I., 2007. Stress, strain, and B-type olivine fabric in the fore-arc mantle: Sensitivity tests using high-resolution steady-state subduction zone models. *J. Geophys. Res.* 112 (B4), 1978–2012.
- Kneller, E.A., van Keken, P.E., 2008. Effect of three-dimensional slab geometry on deformation in the mantle wedge: Implications for shear wave anisotropy. *Geochem. Geophys. Geosyst.* 9, Q01003. <http://dx.doi.org/10.1029/2007GC001677>.
- Le Pichon, X., Angelier, J., 1979. The Hellenic arc and trench system: A key to the neotectonic evolution of the eastern Mediterranean Area. *Tectonophysics* 60, 1–42. [http://dx.doi.org/10.1016/0040-1951\(79\)90131-8](http://dx.doi.org/10.1016/0040-1951(79)90131-8).
- Li, Z.-H., Ribe, N.M., 2012. Dynamics of free subduction from 3-D boundary element modeling. *J. Geophys. Res.* 117. <http://dx.doi.org/10.1029/2012JB009165>.
- Long, M.D., Becker, T.W., 2010. Mantle dynamics and seismic anisotropy. *Earth Planet. Sci. Lett.* 297. <http://dx.doi.org/10.1016/j.epsl.2010.06.036>.
- Long, M.D., Silver, P.G., 2009. Mantle flow in subduction systems: The sub-slab flow field and implications for mantle dynamics. *J. Geophys. Res.* 114. <http://dx.doi.org/10.1029/2008JB006200>.
- McKenzie, D., 1978. Active tectonics of the Alpine–Himalayan belt: The Aegean Sea and surrounding regions. *Geophys. J. R. Astron. Soc.* 55 (1), 217–254.
- McKenzie, D., 1979. Finite deformation during fluid flow. *Geophys. J. R. Astron. Soc.* 58, 689–715.
- Molnar, P., 1988. Continental tectonics in the aftermath of plate tectonics. *Nature* 335, 131–137.
- Monteiller, V., Chevrot, S., 2010. How to make robust splitting measurements for single-station analysis and three-dimensional imaging of seismic anisotropy. *Geophys. J. Int.* 182, 311–328. <http://dx.doi.org/10.1111/j.1365-246X.2010.04608.x>.
- Nishimura, C.E., Forsyth, D.W., 1989. The anisotropic structure of the upper mantle in the Pacific. *Geophys. J. Int.* 96, 203–229. <http://dx.doi.org/10.1111/j.1365-246X.1989.tb04446.x>.

- Papazachos, B.C., Karakostas, B., Papazachos, C.B., Scordilis, E., 2000. The geometry of the Wadati–Benioff Zone and lithospheric kinematics in the Hellenic arc. *Tectonophysics* 319, 275–300. [http://dx.doi.org/10.1016/S0040-1951\(99\)00299-1](http://dx.doi.org/10.1016/S0040-1951(99)00299-1).
- Pearce, F.D., Rondenay, S., Sachpazi, M., Charalampakis, M., Royden, L.H., 2012. Seismic investigation of the transition from continental to oceanic subduction along the western Hellenic Subduction Zone. *J. Geophys. Res.* 117 (B07306). <http://dx.doi.org/10.1029/2011JB009023>.
- Pérouse, E., Chamot-Rooke, N., Rabaute, A., Briole, P., Jouanne, F., Georgiev, I., Dimitrov, D., 2012. Bridging onshore and offshore present-day kinematics of central and eastern Mediterranean: Implications for crustal dynamics and mantle flow. *Geochem. Geophys. Geosyst.* 13 (Q09013). <http://dx.doi.org/10.1029/2012GC004289>.
- Piomallo, C., Morelli, A., 2003. P wave tomography of the mantle under the Alpine–Mediterranean area. *J. Geophys. Res.* 108. <http://dx.doi.org/10.1029/2002JB001757>.
- Piomallo, C., Becker, T.W., Funicello, F., Faccenna, C., 2006. Three-dimensional instantaneous mantle flow induced by subduction. *Geophys. Res. Lett.* 33. <http://dx.doi.org/10.1029/2005GL025390>.
- Polet, J., Silver, P.G., Beck, S., Wallace, T., Zandt, G., Ruppert, S., Kind, R., Rudloff, A., 2000. Shear wave anisotropy beneath the Andes from the BANJO, SEDA, and PISCO experiments. *J. Geophys. Res.* 105 (B3), 6287–6304.
- Royden, L.H., 1993. The tectonic expression of slab pull at continental convergent boundaries. *Tectonics* 12, 303–325.
- Royden, L.H., Papanikolaou, D.J., 2011. Slab segmentation and late Cenozoic disruption of the Hellenic arc. *Geochem. Geophys. Geosyst.* 12. <http://dx.doi.org/10.1029/2010GC003280>.
- Russo, R.M., Silver, P.G., 1994. Trench-parallel flow beneath the Nazca Plate from seismic anisotropy. *Science* 263. <http://dx.doi.org/10.1126/science.1150809>.
- Schellart, W.P., 2004. Kinematics of subduction and subduction-induced flow in the upper mantle. *J. Geophys. Res.* 109 (B7), 1978–2012.
- Schellart, W.P., Freeman, J., Stegman, D.R., Moresi, L., May, D., 2007. Evolution and diversity of subduction zones controlled by slab width. *Nature* 446 (7133), 308–311.
- Schellart, W.P., Stegman, D.R., Farrington, R.J., Moresi, L., 2011. Influence of lateral slab edge distance on plate velocity, trench velocity, and subduction partitioning. *J. Geophys. Res.* 116 (B10408). <http://dx.doi.org/10.1029/2011JB008535>.
- Silver, P.G., Chan, W.W., 1991. Shear wave splitting and subcontinental mantle deformation. *J. Geophys. Res.* 96 (B10), 16429–16454.
- Song, T.-R.A., Kawakatsu, H., 2012. Subduction of oceanic asthenosphere: Evidence from sub-slab seismic anisotropy. *Geophys. Res. Lett.* 39. <http://dx.doi.org/10.1029/2012GL052639>.
- Song, T.-R.A., Kawakatsu, H., 2013. Subduction of oceanic asthenosphere: A critical appraisal in central Alaska. *Earth Planet. Sci. Lett.* 367, 82–94.
- Soto, G.L., Ni, J.F., Grand, S.P., Sandvol, E., Valenzuel, R.W., Speziale, M.G., Gomez Gonzalez, J.M., Reyes, T.D., 2009. Mantle flow in the Rivera–Cocos subduction zone. *Geophys. J. Int.* 179, 1004–1012.
- Spakman, W., Wortel, M.J.R., Vlaar, N.J., 1988. The Hellenic subduction zone: a tomographic image and its geodynamic implications. *Geophys. Res. Lett.* 15 (1), 60–63.
- Stegman, D.R., Freeman, J., Schellart, W.P., Moresi, L., May, D., 2006. Influence of trench width on subduction hinge retreat rates in 3-D models of slab rollback. *Geochem. Geophys. Geosyst.* 7 (3), Q03012.
- Suckale, J., Rondenay, S., Sachpazi, M., Charalampakis, M., Hosa, A., Royden, L.H., 2009. High-resolution seismic imaging of the Western Hellenic subduction zone using teleseismic scattered waves. *Geophys. J. Int.* <http://dx.doi.org/10.1111/j.1365-246X.2009.04170.x>.
- Wagner, L.S., Fouch, M.J., James, D.E., Long, M.D., 2013. The role of hydrous phases in the formation of trench parallel anisotropy: Evidence from Rayleigh waves in Cascadia. *Geophys. Res. Lett.* 40, 2642–2646. <http://dx.doi.org/10.1002/grl.50525>.
- Wolfe, C.J., Silver, P.G., 1998. Seismic anisotropy of oceanic upper-mantle: shear wave splitting methodologies and observations. *J. Geophys. Res.* 103 (B1), 749–771.
- Wortel, M.J.R., Spakman, W., 2000. Subduction and Slab Detachment in the Mediterranean–Carpathian Region. *Science* 290 (5948), 1910–1917. <http://dx.doi.org/10.1126/science.290.5498.1910>.
- Zandt, G., Humphreys, E., 2008. Toroidal mantle flow through the western U.S. slab window. *Geology* 36, 295–298. <http://dx.doi.org/10.1130/G24611A.1>.